Predicting Frictional Properties of Graphene Kirigami Using Molecular Dynamics and Neural Networks

Designs for a negative friction coefficient

Mikkel Metzsch Jensen

Thesis submitted for the degree of
Master in Computational Science: Materials Science
60 credits

Department of Physics
Faculty of mathematics and natural sciences

UNIVERSITY OF OSLO

Spring 2023

Predicting Frictional Properties of Graphene Kirigami Using Molecular Dynamics and Neural Networks

Designs for a negative friction coefficient

Mikkel Metzsch Jensen

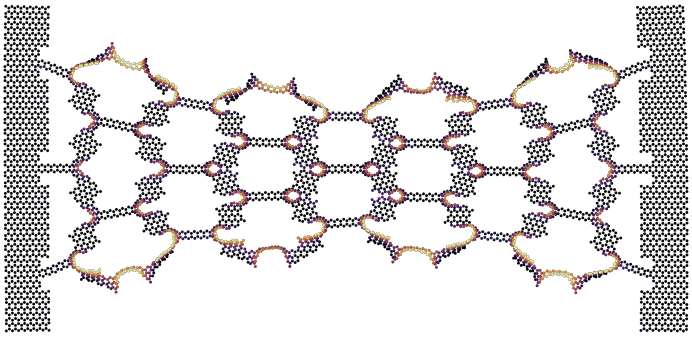

Predicting Frictional Properties of Graphene Kirigami Using Molecular Dynamics and Neural Networks

http://www.duo.uio.no/

Printed: Reprosentralen, University of Oslo

Abstract

Various theoretical models and experimental results propose different governing mechanisms for friction at the nanoscale. We consider a graphene sheet modified with Kirigami-inspired cuts and under the influence of strain. Prior research has demonstrated that this system exhibits out-of-plane buckling, which could result in a decrease in contact area when sliding on a substrate. According to asperity theory, this decrease in contact area is expected to lead to a reduction of friction. However, to the best of our knowledge, no previous studies have investigated the friction behavior of a nanoscale Kirigami graphene sheet under strain. Here we show that specific Kirigami designs yield a non-linear dependency between kinetic friction and the strain of the sheet. Using molecular dynamics simulations, we have found a non-monotonic increase in friction with strain. We found that the friction-strain relationship does not show any clear dependency on contact area which contradicts asperity theory. Our findings suggest that the effect is associated with the out-of-plane buckling of the graphene sheet and we attribute this to a commensurability effect. By mimicking a load-strain coupling through tension, we were able to utilize this effect to demonstrate a negative friction coefficient on the order of -0.3 for loads in the range of a few nN. In addition, we have attempted to use machine learning to capture the relationship between Kirigami designs, load, and strain, with the objective of performing an accelerated search for new designs. Although this approach yielded some promising results, we conclude that further improvements to the dataset are necessary in order to develop a reliable model. We anticipate our findings to be a starting point for further investigations of the underlying mechanism for the frictional behavior of a Kirigami sheet. For instance, the commensurability hypothesis could be examined by varying the sliding angle in simulations. We propose to use an active learning strategy to extend the dataset for the use of machine learning to assist these investigations. If successful, further studies can be done on the method of inverse design. In summary, our findings suggest that the application of nanoscale Kirigami can be promising for developing novel friction-control strategies.

Acknowledgments

The task of writing a master's thesis is a demanding and extensive project which I could not have done without the support of many good people around me. First of all, I want to thank my supervisors Henrik Andersen Sveinsson and Anders Malthe-Sørenssen for the assistance in this thesis work. I am especially grateful for the weekly meetings with Henrik and the inspiring discussions had as we unraveled the discoveries related to the topic of this thesis. I remember that I initially asked for an estimate of how much time he had available for supervision and the answer was something along the lines of "There are no limits really, just send me an email and we figure it out". This attitude captures the main experience I have had working with Henrik and I am profoundly grateful for the time and effort he has put into this project. I hope that he did not regret this initial statement too much, because I have certainly been taken advantage of it. I also want to thank Even Marius Nordhagen for technical support regarding the use of the computational cluster. In that context, I also want to acknowledge the Center for Computing in Science Education (CCSE) for making these resources available.

I would like to express my gratitude to all the parties involved in making it possible for me to write my thesis from Italy. I am particularly grateful for the flexibility shown by my supervisors and for the support of Anders Kvellestad, who allowed me to work remotely as a group teacher. I would also like to thank Scuola Normale Superiore for providing me with access to their library.

I realize that it is a commonly used cliché to express gratitude for the support of loved ones. However, I want to highlight the exceptional role played by my fiancé, Ida, who deserves the main credit for enabling me to maintain a healthy state of mind. She has provided me with a solid foundation for a fulfilling life that enables me to pursue secondary objectives, such as an academic career. I look forward to spending the rest of my life with you.

In this thesis, I have used the formal pronoun "we" mainly as a customary habit related to the formalities of scientific writing in a team. Nonetheless, I have realized that this usage is more fitting as I have not been working alone on this project. I have received support all the way from colleagues and friends at the University of Oslo, my family residing in Denmark, and my life partner who slept beside me every night here in Italy. They are the "good people around me" who have made this thesis possible.

Acronyms

FFM Friction Force Microscopy. 7

GAN Generative Adversarial Networks. 2

LJ Lennard-Jones. 7, 8, 9, 10

MD Molecular Dynamics. 1, 2, 3, 4, 7, 8, 14, 16

ML Machine Learning. 2

Contents

Chapter 1

Introduction

1.1 Motivation

Friction is the force that prevents the relative motion of objects in contact. In our everyday life, we recognize it as the inherent resistance to sliding motion. Some surfaces appear slippery and some appear rough, and we know intuitively that sliding down a snow-covered hill is much more exciting than its grassy counterpart. Without friction, it would not be possible to walk across a flat surface, lean against the wall without falling over or secure an object by the use of nails or screws [1, p. 5]. It is probably safe to say that the concept of friction is integrated into our everyday life to such an extent that most people take it for granted. However, the efforts to control friction date back to the early civilization (3500 B.C.) with the use of the wheel and lubricants to reduce friction in translational motion [2]. Today, friction is considered a part of the wider field *tribology* derived from the Greek word *tribos* meaning "rubbing". It includes the science of friction, wear and lubrication [2]. The most compelling motivation to study tribology is ultimately to gain full control of friction and wear for various technical applications. Especially, the reduction of friction is of great interest since this can be utilized to improve energy efficiency in mechanical systems with moving parts. Hence, it has been reported that tribological problems have a significant potential for both economic and environmental improvements [3]:

> "On global scale, these savings would amount to 1.4% of the GDP annually and 8.7% of the total energy consumption in the long term." [4].

On the other hand, the reduction of friction is not the only sensible application for tribological studies. Controlling frictional properties, besides minimization, might be of interest in the development of a grasping robot where finetuned object handling is required. While achieving a certain "constant" friction response is readily obtained through appropriate material choices, we are yet to unlock the full capabilities to alter friction dynamically on the go. One example from nature inspiring us to think along these lines is the gecko feet. More precisely, the Tokay gecko has received a lot of attention in scientific studies aiming to unravel the underlying mechanism of its "togglable" adhesion properties. Although the gecko can produce large adhesive forces, it retains the ability to remove its feet from an attachment surface at will [5]. This makes the gecko able to achieve a high adhesion on the feet when climbing a vertical surface while lifting them for the next step remains relatively effortless. For a grasping robot, we might consider an analog frictional concept of a surface material that can change from slippery to rough on demand depending on specific tasks; slippery and smooth when interacting with people and rough and firmly gripping when moving heavy objects.

In recent years an increasing amount of interest has gone into the studies of the microscopic origins of friction, due to the increased possibilities in surface preparation and the development of nanoscale experimental methods. Nano-friction is also of great concern for the field of nano-machining where the frictional properties between the tool and the workpiece dictate machining characteristics [3]. With concurrent progress in computational capacity and development of Molecular Dynamics (MD), numerical investigations serve as an invaluable tool for getting insight into the nanoscale mechanics associated with friction. This simulation-based approach can be considered as a "numerical experiment" enabling us to create and probe a variety of high-complexity systems which are still out of reach for modern experimental methods.

In materials science such MD-based numerical studies have been used to explore the concept of so-called *metamaterials* where the material compositions are designed meticulously to enhance certain physical properties [6–11]. This is often achieved either by intertwining different material types or removing certain regions completely. In recent papers by Hanakata et al. [6, 7], numerical studies have showcased that the mechanical properties of a graphene sheet, yield stress and yield strain, can be altered through the introduction of so-called *Kirigami* inspired cuts into the sheet. Kirigami is a variation of origami where the paper is cut additionally to being folded. While these methods originate as an art form, aiming to produce various artistic objects, they have proven to be applicable in a wide range of fields such as optics, physics, biology, chemistry and engineering [12]. Various forms of stimuli enable direct 2D to 3D transformations through the folding, bending, and twisting of microstructures. While original human designs have contributed to specific scientific applications in the past, the future of this field is highly driven by the question of how to generate new designs optimized for certain physical properties. However, the complexity of such systems and the associated design space makes for seemingly intractable[1] problems ruling out analytic solutions.

Earlier design approaches such as bioinspiration, looking at gecko feet for instance, and Edisonian, based on trial and error, generally rely on prior knowledge and an experienced designer [9]. While the Edisonian approach is certainly more feasible through numerical studies than real-world experiments, the number of combinations in the design space rather quickly becomes too large for a systematic search, even when considering the computation time on modern-day hardware. However, this computational time constraint can be relaxed by the use of machine learning (ML) which has been proven successful in the establishment of a mapping from the design space to physical properties of interest. This gives rise to two new styles of design approaches: One, by utilizing the prediction from a trained network we can skip the MD simulations altogether resulting in an *accelerated search* of designs. This can be further improved by guiding the search according to the most promising candidates. For instance, as done with the *genetic algorithm* based on mutation and crossing. Another more sophisticated approach is through generative methods such as *Generative Adversarial Networks* (GAN) or diffusion models. The latter is being used in state-of-the-art AI systems such as OpenAI's DALL·E2 [13] or Midjourney [14]. By working with a so-called *encoder-decoder* network structure, one can build a model that reverses the prediction process. This is often referred to as *inverse design*, where the model predicts a design based on physical target properties. In the papers by Hanakata et al. [6, 7] both the accelerated search and the inverse design approach was proven successful to create novel metamaterial Kirigami designs with the graphene sheet.

Hanakata et al. attribute the variation in mechanical properties to the non-linear effects arising from the out-of-plane buckling of the sheet. Since it is generally accepted that the surface roughness is of great importance for frictional properties it can be hypothesized that Kirigami-induced out-of-plane buckling can also be exploited for the design of frictional metamaterials. For certain designs, we might hope to find a relationship between the stretching of the sheet and frictional properties. If significant, this could give rise to an adjustable friction beyond the point of manufacturing. For instance, the grasping robot might apply such a material as artificial skin for which stretching or relaxing of the surface could result in a changeable friction strength.

In addition, the Kirigami graphene properties can be explored through a potential coupling between the strain and the normal load, through a nanomachine design, with the aim of altering the friction coefficient. This invites the idea of non-linear friction coefficients which might in principle also take on negative values. This would constitute a rarely found property which is mainly observed for the unloading phase of adhesive surfaces [15] or in the loading phase of particular heterojunction materials [16, 17].

To the best of our knowledge, Kirigami has not yet been implemented to alter the frictional properties of a nanoscale system. However, in a recent paper by Liefferink et al. [18] it is reported that macroscale Kirigami can be used to dynamically control the macroscale roughness of a surface through stretching. They reported that the roughness change led to a changeable frictional coefficient by more than one order of magnitude. This supports the idea that Kirigami designs can be used to alter friction, but we believe that taking this concept to the nanoscale would involve a different set of governing mechanisms and thus contribute to new insight in this field.

1.2 Goals

In this thesis, we investigate the prospects of altering the frictional properties of a graphene sheet through the application of Kirigami-inspired cuts and stretching of the sheet. With the use of molecular dynamics (MD)

[1] In computer science we define an *intractable* problem as a problem with no *efficient* algorithm to solve it nor any analytical solutions. The only way to solve such problems is the *brute-force* approach, simply trying all possible combinations, which is often beyond the capabilities of computational resources.

simulations, we evaluate the frictional properties of various Kirigami designs under different physical conditions. Based on the MD results, we investigate the possibility to use machine learning for the prediction of frictional properties and subsequently using the model for an accelerated search of new designs. The main goals of the thesis can be summarized as follows.

1. Design an MD simulation procedure to evaluate the frictional properties of a Kirigami graphene sheet under specified physical conditions.
2. Develop a numerical tool to generate various Kirigami designs, both by seeking inspiration from macroscale designs and by the use of a random-walk-based algorithm.
3. Investigate the frictional behavior under varying strain and load for different Kirigami designs.
4. Develop and train a machine learning model to predict the MD simulation results and perform an accelerated search of new designs with the goal of optimizing certain frictional properties.

1.3 Contributions

By working towards the goals outlined above (Sec. 1.2), I have discovered a non-linear relationship between the kinetic friction and the strain for certain Kirigami patterns. This phenomenon was found to be associated with the out-of-plane buckling of the Kirigami sheet but with no clear relationship to the contact area or the tension in the sheet. I found that this method does not provide any mechanism for a reduction in friction, in comparison to a non-cut sheet. However, the straining of certain Kirigami sheets allows for a non-monotonic increase in friction. The relationship to normal load was proven negligible in this context and I have demonstrated that a coupled system of load and strain (through sheet tension) can exhibit a negative friction coefficient in certain load ranges. Moreover, I have created a dataset of roughly 10,000 data points for assessing the employment of machine learning and accelerated search of Kirigami designs. I have found, that this approach might be useful, but that it requires an extended dataset in order to produce reliable results for a search of new designs.

During my investigations, I have built three numerical tools, in addition to the usual scripts for data analysis, which are available on Github [19]. The tools are summarized in the following.

- I have written a LAMMPS-based [20] tool for simulating and measuring the frictional properties of a graphene sheet sliding on a substrate. The code is generally made flexible with regard to the choice of sheet configuration, system size, simulation parameters and MD potentials, which makes it applicable for further studies on this topic. I have also built an automized procedure to carry out multiple simulations under varying parameters by submitting jobs to a computational cluster via an ssh connection. This was done by adding minor additions to the Python package developed by E. M. Nordhagen [21].
- I have generated a Python-based tool for generating Kirigami patterns and exporting these in a compatible format with the simulation software created. The generation of molecular structures is done with the use of ASE [22]. Our software includes two classes of patterns inspired by macroscale designs and a random walk algorithm which allows for a variety of different designs through user-defined biases and constraints. Given our system size of choice, the first two pattern generators are capable of generating on the order of 10^8 unique designs while the random walk generator allows for significantly more.
- I have built a machine-learning tool based on Pytorch [23] which includes setting up the data loaders, a convolutional network architecture, a loss function, and general algorithms for training and validating the results. Additionally, I have written several scripts for performing grid searches and analyzing the model predictions in the context of the frictional properties of graphene.

All numerical implementations have been originally developed for this thesis except for the libraries mentioned above along with common Python libraries such as Numpy and Matplotlib.

1.4 Thesis structure

The thesis is divided into two parts. In Part I we introduce the relevant theoretical background, and in Part II we present the numerical implementations and the results of this thesis.

Part I contains a description of the theoretical background related to Friction (**??**), Molecular Dynamics (Chapter 2) and Machine Learning (**??**). In **??** we formulate our research questions in the light of the friction theory.

In Part II, we begin by presenting the system in **??** which includes a definition of the main parts of the system and the numerical procedures related to the MD simulation. Here we also present the generation of Kirigami designs. In **??** we carry out a pilot study where we evaluate the simulation results for various physical conditions and compare a non-cut sheet to two different Kirigami designs. In **??**, we further explore the Kirigami patterns through the creation of a dataset and the employment of machine learning and an accelerated search for new designs. In **??**, we use the results from the pilot study to demonstrate the possibility to achieve a negative friction coefficient for a system with coupled load and strain. Finally, in **??**, we summarize our results and provide an outlook for further studies. Additional figures are shown in **??**, **??** and **??**.

Part I

Background Theory

Chapter 2

Molecular Dynamics

Molecular Dynamics (MD) is an atomistic simulation method that is commonly employed in the investigation of atomic-scale friction due to its ability to track each atom in a system [24]. In recent years, advances in computing algorithms and hardware have made MD simulations increasingly capable of simulating tribological systems [25]. We will utilize MD as our primary numerical approach to examine the frictional behavior of a nanoscale Kirigami sheet sliding on a substrate. The small-scale modifications associated with nanoscale Kirigami are still beyond the reach of experimental approaches, and the complexity of the system precludes analytical solutions as well. Hence, MD simulations represent one of the few viable options for addressing this problem.

An MD simulation can be viewed as a "computational experiment", where we specify a set of initial conditions and evolve the system to measure certain properties of interest. This is done through the definition of interatomic force fields which allow us to solve Newton's equations of motion by numerical integration [26, p. 303]. Other more sophisticated and accurate approaches exist, like ab initio MD which utilizes electronic structure calculations at simulation time [27]. One of the most popular methods is based on density functional theory (DFT) [28] which considers quantum mechanical modeling of the electronic state of the system. However, such methods are rarely used in sliding friction simulations since the computational cost makes it only feasible to handle relatively small systems, typically hundreds of atoms, for relatively short durations, typically much less than 1 ns [29]. In addition, we aim to perform multiple simulations under the change of various physical parameters which adds extra demands on the computational resources.

In this chapter, we introduce the fundamental principles of MD modeling and describe our implementation choices for the system of interest. We will focus on the key aspects related to our implementation rather than providing a comprehensive analysis of all available techniques.

2.1 Potentials

The interatomic force fields governing the MD simulation are given from the choice of potentials and have a significant impact on the outcomes obtained. The potentials can vary from intricate energy surfaces that consider electrons at either the density-functional or tight-binding level to angle-dependent many-particle potentials, basic pairwise potentials, or simple models of elastic springs, and extensions of Frenkel-Kontorova-type formulations [29]. For the choice of potentials, and materials, we take a basis in the numerical MD study by Li et al. [30] simulating a FFM type setup where a silicon tip indents a graphene sheet supported by a silicon substrate. Our system obviously differs from this arrangement since we will be sliding the entire sheet upon the substrate. Nevertheless, we contend that this serves as an appropriate basis for selecting the potentials based on the materials involved. Thus, we adopt the potentials from [30] describing the covalent bonds between carbon atoms (C–C) in the graphene sheet with the Tersoff potential [31] and the covalent bonds between silicon atoms (Si–Si) in the substrate with the Stillinger–Weber potential [32]. A typical 12–6 Lennard–Jones (LJ) potential is used to describe the van der Waals adhesive interaction between the graphene sheet and the substrate.

2.1.1 General formulation of potentials

The potentials determine the interatomic forces in the MD simulation, with the force F acting on an atom being derived from the potential energy U as the derivative $\mathbf{F} = -\nabla U$, where $\nabla = (\frac{\partial}{\partial x}, \frac{\partial}{\partial y}, \frac{\partial}{\partial z})$. The energy of N

interacting particles can be described as an expansion in terms of participating particles as

$$U = \sum_i V_1(\mathbf{r}_i) + \sum_{\substack{i,j \\ i<j}} V_2(\mathbf{r}_i, \mathbf{r}_j) + \sum_{\substack{i,j,k \\ i<j<k}} V_3(\mathbf{r}_i, \mathbf{r}_j, \mathbf{r}_i) + \cdots ,$$

where $\mathbf{r}_n$ is the position of the n^{th} particle and V_m is called an m-body potential [31]. The first one-body term corresponds to an external potential (e.g. gravity), followed by the two-body term, the three-body term and so on. The simplest model that includes particle interaction is the pair potential truncating the expansion after the two-body term. A general feature of the pair potentials is that they favor close-packed structures that are unsuited to describe covalent bonds which take more open structures. In particular, pair potentials are completely inapplicable to strongly covalent systems [31]. In order to accommodate the description of covalent bonds, we include the three-body term in both the Stillinger–Weber and Tersoff potential. For the interaction between the sheet and the substrate, we use the LJ pair potential describing the non-bonded van der Waals interaction which is often used to treat interactions between surfaces in friction simulations [3, 33–35]. In the following sections Sec. 2.1.2 to 2.1.4 we will introduce each of the potentials in more detail.

2.1.2 Lennard Jones

The theoretical basis in this section is based on [36–38]. The Lennard-Jones (LJ) model is one of the most commonly used pair potentials for MD simulations. LJ models the potential energy between two non-bonding atoms solely based on interatomic distance. The model accounts for long-ranged attractive forces arising from London dispersion forces (dipole-induced dipole) and repulsive forces that capture the hard core of overlapping electron orbitals at small distances (Pauli repulsion). Thus, it assumes neutrally charged atoms and was originally proposed for noble gases. The classical 12–6 version of the model, referring to the powers of the repulsive and attractive forces respectively, reads

$$U = 4\epsilon \left[\left(\frac{\sigma}{r}\right)^{12} - \left(\frac{\sigma}{r}\right)^{6} \right], \qquad r < r_c, \tag{2.1}$$

where r is the interatomic distance with cut-off r_c, ϵ is the depth of the potential well and σ the interatomic distance where the the potential is zero. The potential is illustrated in Fig. 2.1. By solving for the potential minimum ($dU/dr = 0$) we find the equilibrium distance to be $r_0 = \sigma 2^{1/6}$. This makes for a slightly more intuitive interpretation of σ as the parameter which sets the equilibrium distance between atoms, i.e. the dividing line for which the force is repulsive or attractive. We will adopt the potential parameters from Li et al. [30] with $\sigma = 3.0\,\text{Å}$ and $\epsilon = 0.0092\,\text{eV}$.

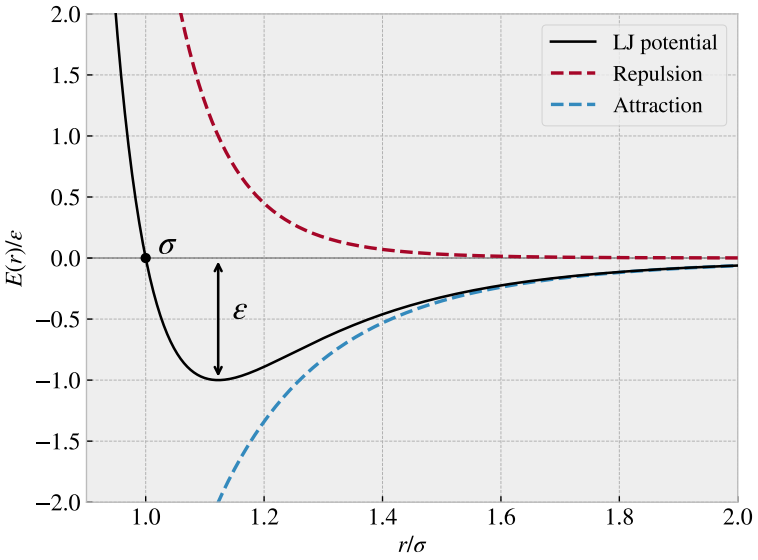

Figure 2.1: Illustration of the LJ potential described by Eq. (2.1) showing the contributions from the repulsive and attractive part of the potential.

2.1.3 Stillinger-Weber

The theoretical background of this section is based on [32, 39]. The Stillinger-Weber potential takes the form of a three-body potential

$$U = \sum_i \sum_{j>i} \phi_2(r_{ij}) + \sum_i \sum_{j\neq i} \sum_{k>j} \phi_3(r_{ij}, r_{ik}, \theta_{ijk}),$$

where r_{ij} denotes the distance between atom i and j, and θ_{ijk} the angle between bond ij and jk (see Fig. 2.2). The first sums run over all pair interactions while the last sums run over triplets of particles, for neighbors j and k of atom i within a cut-off distance $r = a\sigma$.

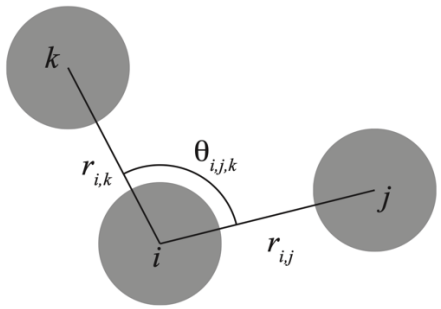

Figure 2.2: Illustration showing the definition of the angle θ_{ijk}.

The two-body term ϕ_2 builds from the LJ model with the addition of an exponential cutoff term

$$\phi_2(r_{ij}) = A_{ij}\epsilon_{ij}\left[B_{ij}\left(\frac{\sigma_{ij}}{r_{ij}}\right)^{p_{ij}} - \left(\frac{\sigma_{ij}}{r_{ij}}\right)^{q_{ij}}\right] \exp\left(\frac{\sigma_{ij}}{r_{ij} - a_{ij}\sigma_{ij}}\right). \tag{2.2}$$

The model parameters A, ϵ, B, σ, p, q and a come with i, j indices to indicate that these parameters should be specified for each unique pair of atom types. However, in our case, we will only provide a single value for each model parameter since we are exclusively dealing with Si–Si bonds. We see that the first term in Eq. (2.2) is reminiscent of the LJ model in Eq. (2.1) while the last term effectively drives the potential to zero at $r = a\sigma$, which is the chosen cut-off distance for the potential evaluation. With the chosen model parameters for the Si–Si bonds (see Table 2.1), the cut-off becomes $\sim 3.8\,\text{Å}$. The three body term includes an angle dependency as

$$\phi_3(r_{ij}, r_{ik}, \theta_{ijk}) = \lambda_{ijk}\ \epsilon_{ijk}\Big[\cos\theta_{ijk} - \cos\theta_{0,ijk}\Big]^2 \exp\left(\frac{\gamma_{ij}\sigma_{ij}}{r_{ij} - a_{ij}\sigma_{ij}}\right) \exp\left(\frac{\gamma_{ik}\sigma_{ik}}{r_{ik} - a_{ik}\sigma_{ik}}\right), \tag{2.3}$$

where $\theta_{0,ijk}$ is the equilibrium angle. The first term of Eq. (2.3) includes an angle dependency analog to a harmonic oscillator based on a cosine angle distance from the equilibrium angle. The final two terms act again as a cut-off function by driving the potential to zero at $r_{ij} = a_{ij}\sigma_{ij}$ and $r_{ik} = a_{ik}\sigma_{ik}$ respectively. We adopt the parameters for the modeling of the Si–Si bonds suggested in the original paper by Stillinger and Weber [32] which is shown in Table 2.1 along with an interpretation of each model parameter.

Table 2.1: Parameters for the Stilliner-Weber potential used for the modeling of the Si–Si bonds in the silicon substrate. The parameters are adopted from [32].

Parameter	Value	Description
ϵ	2.1683 eV	Depth of the potential well for each pair and triplets of atoms.
σ	2.0951 Å	Distance for which the individual pair interactions has zero potential (analog to the LJ model).
a	1.80	The cut-off distance for each pair of atoms in units of σ.
λ	21.0	The overall depth of the three-body potential well.
γ	1.20	Determines the shape of the three-body cut-off terms.
$\cos(\theta_0)$	-1/3	Cosine of the equilibrium angle.
A	7.049556277	The overall depth of the two-body potential well.
B	0.6022245584	Scales the repulsion part of the two-body term.
p	4.0	The power dependency for the repulsion part of the two-body term.
q	0.0	The power dependency for the attraction part of the two-body term.
tol	0	(LAMMPS specific) Option to define a different cut-off than the theoretical $r = a\sigma$. tol = 0 refers to the use of the theoretical cut-off.

2.1.4 Tersoff

The theoretical basis in this section is based on [31, 40]. The Tersoff potential abandons the idea of a general m-body form and attempts instead to build the model on a more physics-informed approach; the more neighbors an atom has the weaker the bonds will be. Thus, it introduces the bond order (bond strength), which is environment specific and decreases with increasing bond coordination (number of neighbors for a given atom). A sketch of the Tersoff potential can be seen in Fig. 2.3.

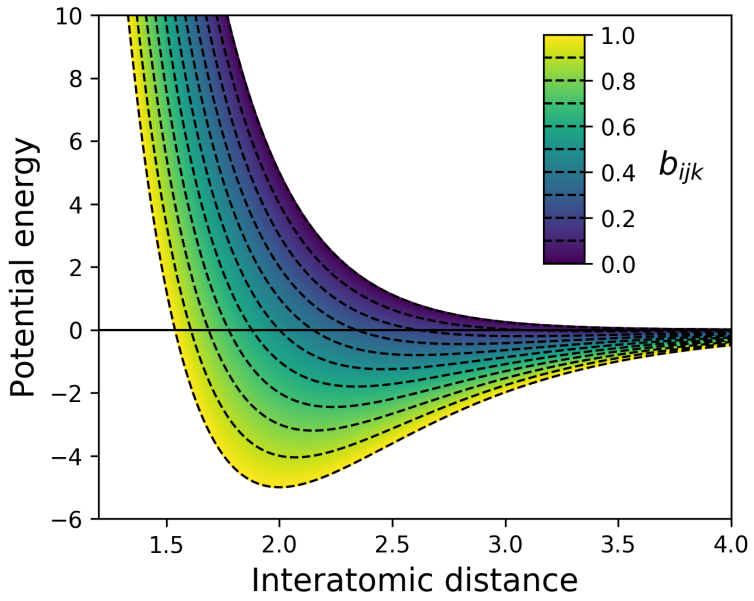

Figure 2.3: Sketch of the potential energy for a Tersoff-type potential. The energy minimum is shifted with changing bond order b_{ijk}. Reproduced from [41].

The potential energy is taken to have the form

$$U = \sum_i U_i = \frac{1}{2}\sum_{i \neq j} V_{ij},$$
$$V_{ij} = f_C(r_{ij})\big[f_R(r_{ij}) + b_{ij} f_A(r_{ij})\big],$$

where the total potential energy U is decomposed into a bond energy V_{ij}. The indices i and j run over the atoms of the system with r_{ij} denoting the distance between atom i and j. Notice that the sum includes all combinations of i, j but $i \neq j$, meaning that an atom cannot bond to itself. However, we count other bonds twice, e.g. $(1, 2)$ and $(2, 1)$, which is the explanation for the additional factor $1/2$. The reasoning for the double counting lies in the asymmetry of the bond order $b_{ij} \neq b_{ji}$ leading to $V_{ij} \neq V_{ji}$. The bond energy is composed of a repulsive term f_R, arising from overlapping wave functions, and an attractive term f_A associated with bonding. f_C is simply a smooth cut-off function to increase computational efficiency. b_{ij} represent the bond order, i.e. the strength of the bonds, which depends inversely on the number of bonds, the bond angles (θ_{ijk}) and optionally the relative bond lengths (r_{ij}, r_{jk}). Notice that an additional cut-off term a_{ij} was originally multiplied to f_R as a way of limiting the range of the repulsive interactions to the first neighbor shell. This is similar to the role of b_{ij} for the attractive term f_A, but it is often omitted for the repulsive term f_R, and we do so as well by setting $a_{ij} = 1$.

The cut-off function f_C goes from 1 to 0 over a small interval range $R \pm D$ as

$$f_C(r) = \begin{cases} 1 & r < R - D \\ \frac{1}{2} - \frac{1}{2}\sin\left(\frac{\pi}{2}\frac{r-R}{D}\right) & R - D < r < R + D \\ 0 & r > R + D \end{cases},$$

which is continuous and differentiable for all r. R is usually chosen to include only the first neighbor shell. The repulsive and attractive terms f_R and f_A are modeled as an exponential function, similar to a Morse potential,

$$f_R(r) = A\exp(-\lambda_1 r),$$
$$f_A(r) = -B\exp\big(-\lambda_2 r\big).$$

The novel feature of the Tersoff model lies in the modeling of the bond order b_{ij} which includes three-body interactions by summing over a third atom $k \neq i, j$ within the cut-off $r_{ik} < R + D$ as shown in the following.

$$b_{ij} = \left(1 + \beta^n \zeta_{ij}^n\right)^{-\frac{1}{2n}} \tag{2.4}$$
$$\zeta_{ij} = \sum_{k \neq i,j} f_C(r_{ik}) g\Big(\theta_{ijk}\left(r_{ij}, r_{ik}\right)\Big) \exp\left(\lambda_3{}^m \big(r_{ij} - r_{ik}\big)^m\right) \tag{2.5}$$
$$g(\theta) = \gamma_{ijk}\left(1 + \frac{c^2}{d^2} - \frac{c^2}{\left[d^2 + (\cos\theta - \cos\theta_0)^2\right]}\right). \tag{2.6}$$

In Eq. (2.6) $\zeta_{i,j}$ is an effective coordination and $g(\theta)$ captures angle dependency and is minimized at the equilibrium angle $\theta = \theta_0$. The parameters used to model the graphene C–C bonds are adopted from J. Tersoff [42] and summarized in Table 2.2.

Table 2.2: Parameters for the Tersoff potential used for the modeling of the C–C bonds in the graphene sheet. The parameters are adopted from [42].

Parameter	Value	Description
R	1.95 Å	Center distance for cut-off.
D	0.15 Å	Thickness of cut-off region.
λ_1	3.4879 Å^{-1}	Decay of repulsion potential term f_R.
λ_2	2.2119 Å^{-1}	Decay of attractive potential term f_A.
A	1393.6 eV	Repulsion potential maximum at the core ($f_R(r_{ij} = 0)$).
B	346.74 eV	Attractive potential minimum at core ($f_A(r_{ij} = 0)$).
β	1.5724×10^{-7}	Base for the exponential scaling of the effective coordination affecting the bond strength b_{ij}.
n	0.72751	Power law exponent for the bond order dependency.
λ_3	0.0 Å^{-1}	Base for the exponential cut-off of the effective coordination ζ_{ij}.
m	—	Exponent for the exponential cut-off of the effective coordination ζ_{ij}. Not relevant since $\lambda_3 = 0$.
γ	1.0	Linear scaling of the angle dependecny term.
c	3.8049×10^4	Strength of the angular effect.
d	4.3484	Determines the "sharpness" of the angular dependency.
$\cos(\theta_0)$	−0.57058	Cosine of the equilibrium angle.

2.2 Integration

Assuming that one has defined a system of atoms, defining the atom types, initial positions and velocities, and interatomic potentials, we need to move the system forward in time. By solving Newton's equations of motion we achieve this by effectively sampling the microcanonical ensemble characterized by a constant number of particles N, volume V and energy E, hence denoted NVE [43]. Newton's equations of motion read

$$m_i \frac{d^2\mathbf{r}_i}{dt^2} = \mathbf{F}_i = -\nabla U_i, \tag{2.7}$$

where i is the atom index, m_i its mass, $\mathbf{r}_i = (x_i, y_i, z_i)$ the position, t is time, $\nabla_i = (\frac{\partial}{\partial x_i}, \frac{\partial}{\partial y_i}, \frac{\partial}{\partial z_i})$ and U_i the potential energy. The potential energy is defined by the interatomic potentials and any external forces applied to the system. Since the forces defined by the potentials are conservative we expect the energy of the solution to be conserved. We can redefine Eq. (2.7) in terms of two coupled first order differential equations

$$\dot{\mathbf{v}}_i(t) = \frac{\mathbf{F}}{m_i}, \qquad \dot{\mathbf{r}}_i(t) = \mathbf{v}_i(t), \tag{2.8}$$

where $\dot{x} = dx/dt$ is Newton's notation for the time derivative and $\mathbf{v} = (v_x, v_y, v_z)$ is velocity. Numerically we can solve the coupled equations by integrating over discrete timesteps. That is, we discretize the solution into temporal steps $t_k = t_0 + k\Delta t$, $k = 0, 1, \ldots, (T - t_0)/\Delta t$ with start time t_0, timestep Δt and total time T. The choice of timestep should be chosen small enough to avoid instabilities in the numerical solution.

2.2.1 Velocity Verlet

A popular approach to the numerical integration of Newton's equations of motion, when written as two coupled first-order differential equations Eq. (2.8), is the *velocity verlet* algorithm. We can derive the algorithm by the use of Taylor expansions. We begin by expanding the next-step position vector $\mathbf{r}_i(t + \Delta t)$ at time t

$$\mathbf{r}_i(t + \Delta t) = \mathbf{r}_i(t) + \dot{\mathbf{r}}_i(t)\Delta t + \frac{\ddot{\mathbf{r}}_i(t)}{2}\Delta t^2 + \mathscr{O}(\Delta t^3), \tag{2.9}$$

where $\ddot{\mathbf{r}} = d^2\mathbf{r}/dt^2$ and Δt^n is simply the relaxed notation for $(\Delta t)^n$. The remaining term $\mathscr{O}(\Delta t^3)$ is big O notation for the truncation including a dependence of Δt^3 and higher order. Similarly, we take the expansions of

the next-step velocity vector $\mathbf{v}_i(t+\Delta t)$ at time t

$$\mathbf{v}_i(t+\Delta t) = \mathbf{v}_i(t) + \dot{\mathbf{v}}_i(t)\Delta t + \frac{\ddot{\mathbf{v}}_i(t)}{2}\Delta t^2 + \mathscr{O}(\Delta t^3). \tag{2.10}$$

Finally, by taking the expansion of $\dot{\mathbf{v}}_i(t+\Delta t)$ we can eliminate the $\ddot{\mathbf{v}}_i$-term in Eq. (2.10) and simplify it as shown in the following.

$$\begin{aligned}
\dot{\mathbf{v}}_i(t+\Delta t) &= \dot{\mathbf{v}}_i(t) + \ddot{\mathbf{v}}_i(t)\Delta t + \mathscr{O}(\Delta t^2) \\
\frac{\ddot{\mathbf{v}}_i(t)}{2}\Delta t^2 &= \frac{\Delta t}{2}\Big(\dot{\mathbf{v}}(t+\Delta t) - \dot{\mathbf{v}}_i(t)\Big) + \mathscr{O}(\Delta t^3) \\
&\Downarrow \\
\mathbf{v}_i(t+\Delta t) &= \mathbf{v}_i(t) + \dot{\mathbf{v}}_i(t)\Delta t + \frac{\Delta t}{2}\Big(\dot{\mathbf{v}}_i(t+\Delta t) - \dot{\mathbf{v}}_i(t)\Big) + \mathscr{O}(\Delta t^3) \\
&= \mathbf{v}_i(t) + \frac{\Delta t}{2}\Big(\dot{\mathbf{v}}_i(t) + \dot{\mathbf{v}}_i(t+\Delta t)\Big) + \mathscr{O}(\Delta t^3).
\end{aligned} \tag{2.11}$$

By combining Eq. (2.9) and Eq. (2.11) using $\dot{\mathbf{v}} = \mathbf{F}_i(t)/m_i$ and $\mathbf{v} = \dot{\mathbf{r}}$ we arrive at the final scheme

$$\begin{aligned}
\mathbf{r}_i(t+\Delta t) &= \mathbf{r}_i(t) + \mathbf{v}_i(t)\Delta t + \frac{\mathbf{F}_i(t)}{2m_i}\Delta t^2 + \mathscr{O}(\Delta t^3), \\
\mathbf{v}_i(t+\Delta t) &= \mathbf{v}_i(t) + \frac{\mathbf{F}_i(t) + \mathbf{F}_i(t+\Delta t)}{2m_i}\Delta t + \mathscr{O}(\Delta t^3).
\end{aligned}$$

This scheme will give a local error on the order Δt^3 corresponding to a global error on the order Δt^2. One of the most popular ways to implement this numerically is as stated in the following steps.

1. Calculate $v_{k+\frac{1}{2}} = v_k + \frac{F_k}{2m}\Delta t$.
2. Calculate $r_{k+1} = r_k + v_{k+\frac{1}{2}}\Delta t$.
3. Evaluate the force $F_{k+1} = F(r_{k+1})$.
4. Calculate $v_{k+1} = v_{k+\frac{1}{2}} + \frac{F_{k+1}}{2m}\Delta t$.

2.3 Thermostats

In **??** we introduced friction as an ultimate result of the equipartition theorem stating that the kinetic energy supplied by the sliding motion will tend to transfer to other degrees of freedom and eventually dissipate to the environment as heat through phonon transport (and electrons for a metallic system) [25]. However, when modeling the system exclusively through the solutions of Newton's equations of motion we have no dissipation channel in our system. Instead, the energy will reflect back and forth and eventually "pile up" in the system in an unphysical manner. In order to resolve this issue we have to model the heat dissipation to the environment. This can be approached in a variety of ways, but one of the more common choices, which we will use as well, is the Langevin thermostat.

2.3.1 Langevin thermostat

The Langevin thermostat is a stochastic thermostat that modifies Newton's equations of motion such that the solution lies in the canonical ensemble characterized by a constant number of particles N, constant volume V and constant temperature T, hence denoted NVT [25]. When going from the microcanonical ensemble NVE, described by Newton's equations of motion Eq. (2.7), to the canonical ensemble NVT, we effectively perform a Legendre transformation which substitutes temperature for energy in the regard to which variables are held constant. The canonical ensemble is represented by a finite system being in contact with an infinite heat bath of temperature T. The NVT ensemble is equivalent to sampling a system in thermodynamic equilibrium where the weight of each microscopic state is given by the Boltzmann factor $\exp[-E/(k_B T)]$ where k_B is the Boltzmann constant.

The Langevin thermostat is governed by the Langevin equation which originated as the modified version of Newton's equations for a Brownian particle [44]. A Brownian particle is a small particle suspended in liquid, e.g. pollen or dust, named after Robert Brown (1773–1858) who was the first to observe its jittery motion. The Langevin equation describes this motion as the combination of a viscous drag force $-\alpha\mathbf{v}$, where α is a positive friction coefficient and $\mathbf{v}$ the velocity vector, and a random fluctuation force $\mathbf{R}$. The Langevin equation reads

$$m\frac{d\mathbf{v}}{dt} = -\alpha\mathbf{v} + \mathbf{R}, \tag{2.12}$$

where m is the particle mass. This effectively describes the particle of interest, the Brownian particle, as being suspended in a sea of smaller particles. The collision with these smaller particles is then modeled by the combined effects of the drag force and the fluctuation force. If the fluctuation force is excluded Eq. (2.12) becomes

$$m\frac{d\mathbf{v}}{dt} = -\alpha\mathbf{v} \quad \Rightarrow \quad \mathbf{v}_i(t) = v(0)e^{-\frac{\alpha t}{m}},$$

where the solution reveals that the Brownian particle will come to a complete stop after a long time $\mathbf{v}_i(t \to \infty) \to \mathbf{0}$. This is in violation with the equipartition theorem which dictates a non-zero average squared velocity in equilibrium $\langle v^2 \rangle_{\text{eq}}$ as

$$\frac{1}{2}m\langle v^2 \rangle_{\text{eq}} = \frac{k_B T}{2}. \tag{2.13}$$

Hence, the fluctuation force is necessary to obtain the correct equilibrium. In the following, we will attempt to introduce the reasoning behind the Langevin equation using only one dimension in order to simplify the notation a bit. The theoretical basis in this section is based on [44].

We describe the statistical nature of the collisions as a sum of independent momentum transfers

$$\Delta P = \sum_i^N \delta p_i,$$

where ΔP denotes the change of momentum after N momentum transfers δp_i from the environment to the Brownian particle. We assume the first and second moments to be $\langle \delta p \rangle = 0$ and $\langle \delta p \rangle = \sigma^2$. When N is large the central limit theorem states that the random variable ΔP has a gaussian distribution with $\langle P \rangle = 0$ and $\langle \Delta P^2 \rangle = N\sigma^2$. If we consider the momentum change ΔP over a discrete time Δt, where the number of collisions is proportional to time $N \propto \Delta t$, the corresponding fluctuation force $R = \Delta P/\Delta t$ will have a variance

$$\langle R^2 \rangle = \frac{\langle \Delta P^2 \rangle}{\Delta t^2} = \frac{N\sigma^2}{\Delta t^2} \propto \frac{1}{\Delta t}.$$

In an MD simulation, we pick a random force $R(t)$ from a Gaussian distribution every timestep Δt. These random forces will not be correlated as long as Δt is larger than the correlation time from the molecular fluid, which we will assume here. However, there exist corrections to this approximation, but we will not consider these for our scope. By assuming that this criterion is met, we can write the correlation function as

$$\langle R(t)R(0) \rangle = \begin{cases} \frac{a}{\Delta t}, & |t| < \Delta t/2 \\ 0, & |t| > \Delta t/2, \end{cases} \tag{2.14}$$

where the constant a describes the magnitude of the fluctuations. We could in principle determine a from the variance of ΔP, but instead, we will determine it from the equipartition principle. In the limit $\Delta t \to 0$ the correlation function becomes

$$\langle R(t)R(0) \rangle = a\delta(t), \tag{2.15}$$

where δ denotes the Dirac delta function. This is valid for all spatial coordinates which are all independent of each other. Since both the drag force and the fluctuation force originate from the molecular fluid, where the drag force $-\alpha\mathbf{v}$ carries a velocity dependency, it is reasonable to assume that fluctuation force is independent of velocity, i.e. $\langle R_i v_j \rangle = 0$ for all cartesian indices i and j. We can justify the physical motivation for the Langevin equation by determining the relationship between the drag coefficient α and the random force R [44]. From the

Langevin equation Eq. (2.12) we can compute the velocity autocorrelation function. Note that we continue to use only one dimension for simplicity. We begin by multiplying by $(e^{\alpha t/m})/m$

$$\dot{v}(t)e^{\alpha t/m} + \frac{\alpha}{m}v(t)e^{\frac{\alpha t}{m}} = \frac{F}{m}e^{\frac{\alpha t}{m}}.$$

We integrate from $t = -\infty$, using integration by parts on the latter term on the left-hand side, in order to calculate the velocity

$$\int_{-\infty}^{t} dt'\ \dot{v}(t')e^{\frac{\alpha t'}{m}} + \frac{\alpha}{m}v(t')e^{\frac{\alpha t'}{m}} = \int_{-\infty}^{t} dt'\ e^{\frac{\alpha t'}{m}}\frac{F(t')}{m}$$

$$\int_{-\infty}^{t} dt'\ \dot{v}(t')e^{\frac{\alpha t'}{m}} + \left(\left[v(t')e^{\frac{\alpha t'}{m}}\right]_{-\infty}^{t} - \int_{-\infty}^{t} dt'\ \dot{v}(t')e^{\frac{\alpha t'}{m}}\right) = \int_{-\infty}^{t} dt'\ e^{\frac{\alpha t'}{m}}\frac{F(t')}{m}$$

$$v(t) = \int_{-\infty}^{t} dt'\ e^{\frac{-\alpha(t-t')}{m}}\frac{F(t')}{m},$$

where $e^{\frac{-\alpha t}{m}}$ plays the role of a response function. We can then calculate the autocorrelation

$$\begin{aligned}\langle v(t)v(0)\rangle &= \int_{-\infty}^{t} dt_1 \int_{-\infty}^{0} dt_2\ e^{\frac{-\alpha(t-t_1-t_2)}{m}}\frac{\langle F(t_1)F(t_2)\rangle}{m^2}\\ &= \int_{-\infty}^{t} dt_1 \int_{-\infty}^{0} dt_2\ e^{\frac{-\alpha(t-t_1-t_2)}{m}}\frac{a\delta(t_1-t_2)}{m^2}\\ &= \int_{-\infty}^{0} dt_2\ e^{\frac{-\alpha(t-2t_2)}{m}}\frac{a}{m^2} = \frac{a}{2m\alpha}e^{-\frac{\alpha t}{m}},\end{aligned}$$

where we used Eq. (2.15) and the fact that the integration commutes with the average (we are allowed to flip the order). By comparing this with the equipartition theorem we get

$$\frac{1}{2}m\langle v^2\rangle = \frac{k_BT}{2}$$

$$\frac{1}{2}m\langle v(0)v(0)\rangle = \frac{a}{4\alpha} = \frac{k_BT}{2}$$

$$a = 2\alpha k_BT.$$

We notice the appearance of α meaning that the magnitude of the random force fluctuations a increase both with viscous friction $(-\alpha\mathbf{v})$ and temperature T. Moreover, we can integrate the velocity over time to get displacement $x(t)$ and show that the variance is [44]

$$\langle x^2(t)\rangle = \frac{2k_BT}{\alpha}\left(t - \frac{m}{\alpha}\left(1 - e^{-\alpha t/m}\right)\right).$$

For $t \gg m/\alpha$, only the t-term will survive yielding

$$\langle x^2(t)\rangle = 2k_BTt/\alpha.$$

In 1D, the diffusion constant D is related to the variance as $\langle x^2\rangle = 2Dt$, meaning that this represents the Einstein relation $D = \mu k_BT$ with the mobility $\mu = 1/\alpha$. When $t \ll m/\alpha$, we use the Taylor expansion $1 - e^{-x} \approx x - x^2/2$ for $x \ll 1$ which gives

$$\langle x^2(t)\rangle = \frac{k_BT}{m}t^2.$$

Using $\langle x^2\rangle/t^2 = \langle v^2\rangle$ we see that the result is in agreement with the equipartition theorem Eq. (2.13)

$$\langle v^2(t)\rangle = \frac{k_BT}{m} \iff \frac{1}{2}m\langle v^2\rangle_{\text{eq}} = \frac{k_BT}{2}.$$

Thus, we find the finite damping correlation time α/m to describe the crossover between the ballistic regime $\sqrt{\langle x^2(t)\rangle} \propto t$ at $t \ll m/\alpha$ to the diffusive regime $\sqrt{\langle x^2(t)\rangle} \propto \sqrt{t}$ at $t \gg m/\alpha$. That is, at short time scales the thermal movement can be thought of as relatively free with a low collision rate, while at longer time scales the movement is characterized by a jittery random-walk-looking motion that is related to diffusion.

2.3.2 Applying the Langevin Thermostat

The numerical implementation of the Langevin equation Eq. (2.12) is done through the simulation software LAMMPS (see Sec. 2.5) following [45] by defining the force vector for each particle as

$$\begin{aligned}\mathbf{F} &= \mathbf{F_c} + \mathbf{F}_f + \mathbf{F}_r \\ &= -\nabla U - \gamma m \mathbf{v} + \sqrt{\frac{2k_B T m\gamma}{\Delta t}}\mathbf{h}(t),\end{aligned} \tag{2.16}$$

where $\mathbf{F_c}$ is the added conservative force computed via the usual interatomic interactions described by the potential U, $\mathbf{F}_f$ is the drag force described as a damping term $-\gamma m\mathbf{v}$ with $\alpha = \gamma m$, and $\mathbf{F}_r$ is the random fluctuation force where $\mathbf{h}$ is a random vector drawn from a normal distribution with zero mean and unit variance. The fact that Δt now appears in the denominator for the random force variance $2k_BTm\gamma/\Delta t$ is due to the discretization of time. By applying Eq. (2.16) we get the refined velocity verlet scheme

$$\begin{aligned}\mathbf{v}_i(t+\Delta t/2) &= \mathbf{v}_i(t) - \frac{\Delta t}{2}\left(\frac{\nabla_i U(t)}{m_i} + \gamma \mathbf{v}_i\right) + \sqrt{\frac{k_B T\gamma \Delta t}{2m_i}}\mathbf{h}_i, \\ \mathbf{r}_i(t+\Delta t) &= \mathbf{r}_i(t) + \mathbf{v}_i(t+\Delta t/2)\Delta t, \\ \mathbf{v}_i(t+\Delta t) &= \mathbf{v}_i(t+\Delta t/2) - \frac{\Delta t}{2}\left(\frac{\nabla_i U(t+\Delta t)}{m_i} + \gamma \mathbf{v}_i(t+\Delta t/2)\right) + \sqrt{\frac{k_B T\gamma \Delta t}{2m_i}}\mathbf{h}_i,\end{aligned}$$

with new random vector $\mathbf{h}_i$ for each particle and each update. Notice however, we will only apply the thermostat to specific regions in our simulation, mainly on the outer edges, while the main part of interest is modeled exclusively by Newton's equations of motion as described in Eq. (2.7). This is done in order to avoid affecting the governing parts of the friction simulation too much. We use a damping of $1/\gamma = m/\alpha = 1\,\text{ps}$ as a common default choice.

2.4 Limitations

On a general note, MD simulations are limited to relatively small time and size scales due to the available computation time. Modern CPUs perform on the order of 10^9 floating-point operations per second (FLOPS) per core [29]. MD simulations can benefit from medium-scale parallelization, demonstrating relatively linear scaling up to around 10^2 cores, providing roughly 10^{11} FLOPS. In a typical MD calculation, the computation of the force acting on each atom, which can be the most time-consuming step depending on the complexity and range of the force field, requires N_{step} steps being approximately 10 to 10^2 FLOPS. Therefore, for a typical simulation size of $N = 10^5$ atoms with a timestep in the fs range, we find the ratio of simulated time to real-time on the order

$$\frac{\text{FLOPS}}{N \cdot N_{\text{step}} \cdot dt^{-1}} \sim \frac{10^{11}}{10^5 \cdot 10 \cdot 10^{15}} = 10^{-10}.$$

Hence, the simulation can make progress at a rate of 100 ps per second, or roughly 1 μs per day. This serves as a rough estimate for the capabilities of MD simulations. Regarding the "realism" of the simulations, some general weaknesses include the lack of considering quantum effects and a reduction in the number of dissipation channels available.

2.5 LAMMPS

For the implementation of our MD simulations we use LAMMPS (Large-scale Atomic/Molecular Massively Parallel Simulator) [20]. LAMMPS provides a numerical framework for setting up the system and integrating the equations of motion with easy access to parallelization of the simulations. This essentially allows us to focus on the higher-level features of the numerical procedure rather than writing the code from scratch.

Part II

Simulations

Appendices

Bibliography

[1] E. Gnecco and E. Meyer, *Elements of friction theory and nanotribology* (Cambridge University Press, 2015).

[2] Bhusnan, "Introduction", in *Introduction to tribology* (John Wiley & Sons, Ltd, 2013) Chap. 1.

[3] H.-J. Kim and D.-E. Kim, "Nano-scale friction: a review", International Journal of Precision Engineering and Manufacturing **10**, 141–151 (2009).

[4] K. Holmberg and A. Erdemir, "Influence of tribology on global energy consumption, costs and emissions", Friction **5**, 263–284 (2017).

[5] B. Bhushan, "Gecko feet: natural hairy attachment systems for smart adhesion – mechanism, modeling and development of bio-inspired materials", in *Nanotribology and nanomechanics: an introduction* (Springer Berlin Heidelberg, Berlin, Heidelberg, 2008), pp. 1073–1134.

[6] P. Z. Hanakata, E. D. Cubuk, D. K. Campbell, and H. S. Park, "Accelerated search and design of stretchable graphene kirigami using machine learning", Phys. Rev. Lett. **121**, 255304 (2018).

[7] P. Z. Hanakata, E. D. Cubuk, D. K. Campbell, and H. S. Park, "Forward and inverse design of kirigami via supervised autoencoder", Phys. Rev. Res. **2**, 042006 (2020).

[8] L.-K. Wan, Y.-X. Xue, J.-W. Jiang, and H. S. Park, "Machine learning accelerated search of the strongest graphene/h-bn interface with designed fracture properties", Journal of Applied Physics **133**, 024302 (2023).

[9] Y. Mao, Q. He, and X. Zhao, "Designing complex architectured materials with generative adversarial networks", Science Advances **6**, eaaz4169 (2020).

[10] Z. Yang, C.-H. Yu, and M. J. Buehler, "Deep learning model to predict complex stress and strain fields in hierarchical composites", Science Advances **7**, eabd7416 (2021).

[11] A. E. Forte, P. Z. Hanakata, L. Jin, E. Zari, A. Zareei, M. C. Fernandes, L. Sumner, J. Alvarez, and K. Bertoldi, "Inverse design of inflatable soft membranes through machine learning", Advanced Functional Materials **32**, 2111610 (2022).

[12] S. Chen, J. Chen, X. Zhang, Z.-Y. Li, and J. Li, "Kirigami/origami: unfolding the new regime of advanced 3D microfabrication/nanofabrication with "folding"", Light: Science & Applications **9**, 75 (2020).

[13] OpenAI, *Dall-e2*, (2023) `https://openai.com/product/dall-e-2`.

[14] Midjourney, *Midjourney*, (2023) `https://www.midjourney.com`.

[15] Z. Deng, A. Smolyanitsky, Q. Li, X.-Q. Feng, and R. J. Cannara, "Adhesion-dependent negative friction coefficient on chemically modified graphite at the nanoscale", Nature Materials **11**, 1032–1037 (2012).

[16] B. Liu, J. Wang, S. Zhao, C. Qu, Y. Liu, L. Ma, Z. Zhang, K. Liu, Q. Zheng, and M. Ma, "Negative friction coefficient in microscale graphite/mica layered heterojunctions", Science Advances **6**, eaaz6787 (2020).

[17] D. Mandelli, W. Ouyang, O. Hod, and M. Urbakh, "Negative friction coefficients in superlubric graphite–hexagonal boron nitride heterojunctions", Phys. Rev. Lett. **122**, 076102 (2019).

[18] R. W. Liefferink, B. Weber, C. Coulais, and D. Bonn, "Geometric control of sliding friction", Extreme Mechanics Letters **49**, 101475 (2021).

[19] M. Metzsch, *Github repository*, `https://github.com/mikkelme/MastersThesis`.

[20] A. P. Thompson, H. M. Aktulga, R. Berger, D. S. Bolintineanu, W. M. Brown, P. S. Crozier, P. J. in 't Veld, A. Kohlmeyer, S. G. Moore, T. D. Nguyen, R. Shan, M. J. Stevens, J. Tranchida, C. Trott, and S. J. Plimpton, "LAMMPS - a flexible simulation tool for particle-based materials modeling at the atomic, meso, and continuum scales", Comp. Phys. Comm. **271**, 108171 (2022).

[21] E. M. Nordhagen, *LAMMPS simulator*, https://github.com/evenmn/lammps-simulator.

[22] A. H. Larsen, J. J. Mortensen, J. Blomqvist, I. E. Castelli, R. Christensen, M. Dułak, J. Friis, M. N. Groves, B. Hammer, C. Hargus, E. D. Hermes, P. C. Jennings, P. B. Jensen, J. Kermode, J. R. Kitchin, E. L. Kolsbjerg, J. Kubal, K. Kaasbjerg, S. Lysgaard, J. B. Maronsson, T. Maxson, T. Olsen, L. Pastewka, A. Peterson, C. Rostgaard, J. Schiøtz, O. Schütt, M. Strange, K. S. Thygesen, T. Vegge, L. Vilhelmsen, M. Walter, Z. Zeng, and K. W. Jacobsen, "The atomic simulation environment—a python library for working with atoms", Journal of Physics: Condensed Matter **29**, 273002 (2017).

[23] A. Paszke, S. Gross, F. Massa, A. Lerer, J. Bradbury, G. Chanan, T. Killeen, Z. Lin, N. Gimelshein, L. Antiga, A. Desmaison, A. Kopf, E. Yang, Z. DeVito, M. Raison, A. Tejani, S. Chilamkurthy, B. Steiner, L. Fang, J. Bai, and S. Chintala, "Pytorch: an imperative style, high-performance deep learning library", in *Advances in neural information processing systems 32* (Curran Associates, Inc., 2019), pp. 8024–8035.

[24] Y. Dong, A. Vadakkepatt, and A. Martini, "Analytical models for atomic friction", Tribology Letters **44**, 10.1007/s11249-011-9850-2 (2011).

[25] N Manini, O. M. Braun, E Tosatti, R Guerra, and A Vanossi, "Friction and nonlinear dynamics", Journal of Physics: Condensed Matter **28**, 293001 (2016).

[26] B. Bhushan, "Nanotribology and nanomechanics", Wear **259**, 15th International Conference on Wear of Materials, https://doi.org/10.1016/j.wear.2005.01.010 (2005).

[27] P. Carloni, U. Rothlisberger, and M. Parrinello, "The Role and Perspective of Ab Initio Molecular Dynamics in the Study of Biological Systems", Accounts of Chemical Research **35**, Publisher: American Chemical Society, 455–464 (2002).

[28] P. Hohenberg and W. Kohn, "Inhomogeneous electron gas", Phys. Rev. **136**, B864–B871 (1964).

[29] A. Vanossi, N. Manini, M. Urbakh, S. Zapperi, and E. Tosatti, "Modeling friction: from nanoscale to mesoscale", Reviews of Modern Physics **85**, 529–552 (2013).

[30] S. Li, Q. Li, R. W. Carpick, P. Gumbsch, X. Z. Liu, X. Ding, J. Sun, and J. Li, "The evolving quality of frictional contact with graphene", Nature **539**, Number: 7630, 541–545 (2016).

[31] J. Tersoff, "New empirical approach for the structure and energy of covalent systems", Phys. Rev. B **37**, 6991–7000 (1988).

[32] F. H. Stillinger and T. A. Weber, "Computer simulation of local order in condensed phases of silicon", Phys. Rev. B **31**, 5262–5271 (1985).

[33] P. Zhu and R. Li, "Study of nanoscale friction behaviors of graphene on gold substrates using molecular dynamics", Nanoscale Research Letters **13**, 34 (2018).

[34] Q. Zhang, D. Diao, and M. Kubo, "Nanoscratching of multi-layer graphene by molecular dynamics simulations", Tribology International **88**, 85–88 (2015).

[35] H. M. Yoon, Y. Jung, S. C. Jun, S. Kondaraju, and J. S. Lee, "Molecular dynamics simulations of nanoscale and sub-nanoscale friction behavior between graphene and a silicon tip: analysis of tip apex motion.", Nanoscale **7 14**, 6295–303 (2015).

[36] S. Corporation, *Pair_style lj/cut command*, (Dec. 22, 2022) https://docs.lammps.org/pair_lj.html (visited on 01/24/2023).

[37] X. Wang, S. Ramírez-Hinestrosa, J. Dobnikar, and D. Frenkel, "The lennard-jones potential: when (not) to use it", Phys. Chem. Chem. Phys. **22**, 10624–10633 (2020).

[38] R. Naeem, *Lennard-jones potential*, (Nov. 25, 2022) https://chem.libretexts.org/Bookshelves/Physical_and_Theoretical_Chemistry_Textbook_Maps/Supplemental_Modules_(Physical_and_Theoretical_Chemistry)/Physical_Properties_of_Matter/Atomic_and_Molecular_Properties/Intermolecular_Forces/Specific_Interactions/Lennard-Jones_Potential (visited on 01/24/2023).

[39] S. Corporation, *Pair_style sw command*, (Dec. 22, 2022) https://docs.lammps.org/pair_sw.html (visited on 01/24/2023).

[40] S. Corporation, *Pair_style tersoff command*, (Dec. 22, 2022) https://docs.lammps.org/pair_tersoff.html (visited on 01/24/2023).

[41] W. Commons, *File:bond-order interatomic potential.png — wikimedia commons, the free media repository*, [Online; accessed 02/05/2023], (2023) https://commons.wikimedia.org/wiki/File:Bond-order_interatomic_potential.png.

[42] J. Tersoff, "Modeling solid-state chemistry: interatomic potentials for multicomponent systems", Phys. Rev. B **39**, 5566–5568 (1989).

[43] D. Frenkel and B. Smit, *Understanding molecular simulation: from algorithms to applications*, Second, Vol. 1, Computational Science Series (Academic Press, San Diego, 2002).

[44] F. Ravndal and E. G. Flekkøy, *Statistical physics– a second course*, (Mar. 2019) https://www.uio.no/studier/emner/matnat/fys/FYS4130/v19/pensumliste/stat-phys_2019.pdf.

[45] T. Schneider and E. Stoll, "Molecular-dynamics study of a three-dimensional one-component model for distortive phase transitions", Phys. Rev. B **17**, 1302–1322 (1978).